Journal of Colloid and Interface Science 365 (2012) 289–295

Contents lists available at SciVerse ScienceDirect

Journal of Colloid and Interface Science

www.elsevier.com/locate/jcis

Characterization of bonding between poly(dimethylsiloxane) and cyclic olefin copolymer using corona discharge induced grafting polymerization

Ke Liu [a], Pan Gu [a], Kiri Hamaker [b], Z. Hugh Fan [a,b,*]

[a] Interdisciplinary Microsystems Group, Department of Mechanical and Aerospace Engineering, University of Florida, Gainesville, FL 32611-6250, United States
[b] J. Crayton Pruitt Family Department of Biomedical Engineering, University of Florida, Gainesville, FL 32611-6131, United States

ARTICLE INFO

Article history:
Received 19 July 2011
Accepted 3 September 2011
Available online 10 September 2011

Keywords:
Surface modification
Microfluidic valves
Thermoplastics
Elastomer

ABSTRACT

Thermoplastics have been increasingly used for fabricating microfluidic devices because of their low cost, mechanical/biocompatible attributes, and well-established manufacturing processes. However, there is sometimes a need to integrate such a device with components made from other materials such as polydimethylsiloxane (PDMS). Bonding thermoplastics with PDMS to produce hybrid devices is not straightforward. We have reported our method to modify the surface property of a cyclic olefin copolymer (COC) substrate by using corona discharge and grafting polymerization of 3-(trimethoxysilyl)propyl methacrylate; the modified surface enabled strong bonding of COC with PDMS. In this paper, we report our studies on the surface modification mechanism using attenuated total reflectance Fourier transform infrared spectroscopy (ATR-FTIR), X-ray photoelectron spectroscopy (XPS), atomic force microscopy (AFM) and contact angle measurement. Using this bonding method, we fabricated a three-layer (COC/PDMS/COC) hybrid device consisting of elastomer-based valve arrays. The microvalve operation was confirmed through the displacement of a dye solution in a fluidic channel when the elastomer membrane was pneumatically actuated. Valve-enabled microfluidic handling was demonstrated.

1. Introduction

Microfluidic devices have been used in a wide range of applications, including biological assays, cellular studies, DNA sequencing, protein separation and detection [1]. They have potential advantages of low sample and reagent consumption, high throughput and sensitivity, large surface-to-volume ratio, and other benefits related to miniaturization. A number of devices in the earlier efforts [2–4] were fabricated from silicon or glass substrates while many in the recent works were made from polydimethylsiloxane (PDMS) [5–7]. It is generally accepted that PDMS "is not readily or economically formed in high-throughput production" [8] and thermoplastics are "amenable to mass manufacturing processes that facilitate translation of microscale systems from simple laboratory tools to commercially marketable products" [9].

Each material possesses unique properties that are advantageous for certain applications. For instance, PDMS is very elastic with Young's modulus of ~750 kPa [10], thus it is ideal for device components such as valves and gasket membranes. Quake's research group exploited the property and developed elastomer-based microvalves [6,7]. On the other hand, thermoplastics are rigid, thus it is favorable for parts such as microfluidic substrates and port connectors. The components made from thermoplastics are dimensionally stable and mechanically robust while the feature fidelity and integrity are easier to maintain during replication processes.

To take advantages of different properties of various materials, hybrid devices could be made from different substances to have proper functions in microfluidic devices. For example, several research groups recently reported using a rigid thermoplastic polymer as the supporting substrate while incorporating PDMS-based microvalves to control and manipulate solutions in a device [11–15]. Among thermoplastics, cyclic olefin copolymer (COC), poly(methyl methacylate) (PMMA), polystyrene, and polycarbonate have been used most for fabricating microfluidic devices.

The key step to realize such a hybrid device is to bond PDMS with thermoplastics. The reported methods include oxygen plasma or UV/ozone treatment [12], thermal fusion after plasma or ozone treatment [13], surface modification [14–19], and adhesives [11]. The bonding strength varies from weak reversible bonding [12]

Abbreviations: PDMS, polydimethylsiloxane; COC, cyclic olefin copolymer; PMMA, poly(methyl methacylate); APTES, 3-amionpropyltriethoxysilane; TMSPMA, 3-(trimethoxysilyl)propyl methacrylate; ATR-FTIR, attenuated total reflectance Fourier transform infrared spectroscopy; XPS, X-ray photoelectron spectroscopy; AFM, atomic force microscopy; IEF, isoelectric focusing; PAGE, polyacrylamide gel electrophoresis; ELISA, enzyme-linked immunosorbent assay.

* Corresponding author at: Interdisciplinary Microsystems Group, Department of Mechanical and Aerospace Engineering, University of Florida, Gainesville, FL 32611-6250, United States. Fax: +1 352 392 7303.
E-mail address: hfan@ufl.edu (Z.H. Fan).

0021-9797/$ - see front matter © 2011 Elsevier Inc. All rights reserved.
doi:10.1016/j.jcis.2011.09.004

to strong permanent bonding [14–19]. Chemical modification of the plastic surfaces is the most popular method, resulting in long-lasting, strong bonding between PDMS with thermoplastics. Chemicals used in these efforts are almost exclusively 3-amionpropyltriethoxysilane (APTES) [15–19], though we recently reported bonding PDMS with COC using 3-(trimethoxysilyl)propyl methacrylate (TMSPMA) [14]. The primary difference of TMSPMA from APTES is the additional functional group of acrylate that enables grafting polymerization on plastic surfaces [20,21]. The protocol is briefly described as follows. A COC substrate was treated with corona discharge from a Tesla coil gun, followed by an exposure to TMSPMA. The COC substrate was then placed in contact with a PDMS film after both surfaces had been exposed to corona discharge. After thermal annealing, a hermetical bond was formed between COC and PDMS, confirmed by the bonding strength measurement [14]. Note that this bonding method is also applicable to PDMS/PMMA bonding [14].

In this paper, we report our studies on the mechanism of the surface modification that resulted in COC/PDMS bonding. A number of techniques, including attenuated total reflectance Fourier transform infrared spectroscopy (ATR-FTIR), X-ray photoelectron spectroscopy (XPS), atomic force microscopy (AFM) and contact angle measurement, have been used to characterize the reaction mechanisms and surface properties. Using this bonding method, we fabricated a three-layer (COC/PDMS/COC) hybrid device consisting of elastomer-based valve arrays. The microvalve operation was confirmed through the displacement of a dye solution in fluidic channels when the elastomer membrane was pneumatically actuated. To exemplify their practical use, two microvalve arrays were integrated in a device previously applied for two-dimensional protein separation. Sequential introduction of different solutions to this microfluidic device was realized with the assistance of integrated microvalves. Since microvalve technology is an intimate aspect to fulfill versatile chip performance, we believe that this bonding mechanism would be of great interest to a boarder range of microfluidic applications.

2. Experimental

2.1. Reagents and materials

COC resins (Zeonor 1020R) and 188 μm-thick COC films (Zeonor 1420R) were purchased from Zeon Chemicals (Louisville, KY) while PDMS kits were from Dow Corning (Midland, MI). Ethanol and 3-(trimethoxysilyl)propyl methacrylate (TMSPMA) was obtained from Acros Organics (Fair Lawn, NJ).

2.2. Device fabrication

The protein separation device consists of three layers. The bottom layer is the fluid layer containing microchannels for protein separation. The middle layer is an elastomeric PDMS thin film that functions as the deformation element. The top layer is the control layer containing channels for supplying pneumatic pressure. The COC bottom layer was fabricated using the procedure reported previously [14]. To demonstrate the valve functionality for fluidic manipulation, we used the device presented in Ref. [14] that has a similar microfluidic layout from our previous work [22], in which gel pseudo-valves were used for two-dimensional protein separation [22]. The design of the device is shown in Fig. 1a, consisting of one horizontal channel (IEF channel) and 39 parallel channels (PAGE channels). The total length of horizontal channel (including zigzags) is 4.1 cm, while the vertical channels are 6.5 cm long. All channels are 45 μm deep and 110 μm wide, with an aspect ratio of 0.41.

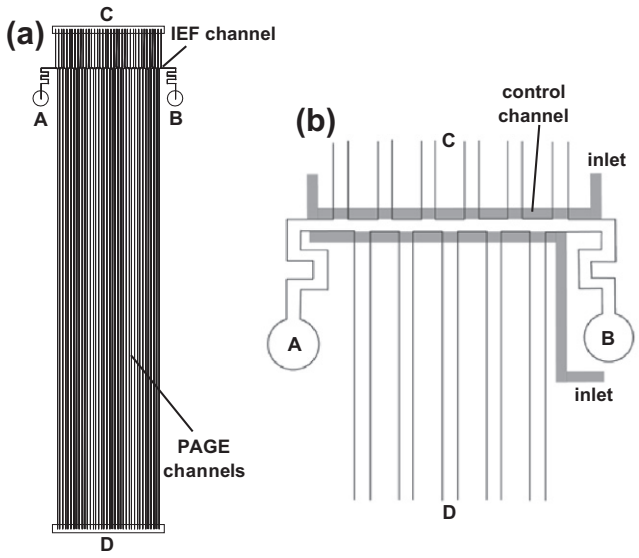

Fig. 1. (a) Layout of the two-dimensional protein separation device containing a horizontal channel AB and vertical channels CD. The size of the device is 1″ × 3″. (b) An exploded view of intersections with a smaller number of channels is shown for simplicity. Channels connecting to reservoir C are staggered with those connecting to reservoir D. Two individually addressable control channels (gray color) are located at each side of the AB channel and they function as a part of microvalves.

The middle PDMS layer was made from prepolymer that was prepared according to the instructions of the manufacturer. The prepolymer was spin-coated at 2500 RPM on a sacrificial plastic layer and then cured, forming a 25-μm-thick PDMS layer. The top layer was fabricated from COC sheet containing control channels with the pattern shown in Fig. 1b. The metal molding die was made in the same way as the bottom layer [23] and the dimension of the resulting control channels was 300 μm wide and 25 μm deep. The distance between two control channels is 110 μm, identical to the width of the IEF channel. An inlet was created at one end of each control channel for supplying pneumatic pressure.

The bonding of PDMS (the middle layer) and COC (the bottom layer) has been described elsewhere [14]. In brief, COC surfaces were activated by exposing to corona discharges, followed by immersing it in TMSPMA solution (6% in ethanol) for 20 min. The COC sheet was taken out from the solution, exposed to a nitrogen stream to remove the excess reagents and solvents, and treated with corona discharges again. The treated COC surfaces were brought into conformal contact with the UV/ozone activated surface of the PDMS layer. The assembly was placed in an oven at 60 °C overnight to reach irreversible bonding.

The top control layer was bonded to the PDMS/COC in a similar fashion. It should be noted that the alignment of the control channels with the central channel is crucial for the performance of the device. Under a microscope, spatial adjustment can be manually completed in a fairly short time after some practices (since the features are in 100's μm).

2.3. Surface characterization

Attenuated total reflection Fourier transform infrared (ATR-FTIR) spectroscopy was used to stepwise investigate the mechanisms of the physical and chemical treatment on the COC surface. All spectra were collected over a range of 650–4000 cm^{-1} in a Magna 760 spectrometer (Thermo Scientific, USA) equipped with a ZnSe ATR unit (Gemini, Spectra Tech). For each spectrum, 64 scans were obtained

at 45° angle of incidence with a resolution of 4 cm^{-1}. The spectrum from a blank ATR cell was used as a reference. The chemical composition on the surface was analyzed using an X-ray photoelectron spectrometer (PHI5100, Perkin Elmer) with a magnesium X-ray source (1253.6 eV). The Mg anode was operated at 20 mA and 15 kV (300 W). The pass energy and take-off angle were 89.5 eV and 45°, respectively. XPS surveys of native and fully processed COC surfaces were obtained and then compared. To confirm the formation of covalent bonds between COC and PDMS, prior to FTIR and XPS analyses, the TMSPMA-grafted COC surfaces were thoroughly rinsed by ethanol and dried to remove unbonded molecules (Figs. 2d and 4a). The washing step was to ensure the removal of the TMSPMA molecules that had been absorbed physically onto the COC surfaces.

Contact angles were measured to study surface wettability and heterogeneity. The experiments were carried out using a goniometer (Ramé-Hart 100-00, Mountain Lakes, NJ) and the advancing contact angles were determined by increasing the volume of a water droplet on the surface of COC via a pipette. Immediately before the contact line started to advance outward, the image of the droplet with a stationary 3-phase boundary was recorded and the advancing contact angle was determined using ImageJ software (National Institution of Health). At least four water droplets on separate substrates were measured and the average value was then reported.

Morphological profiles of native and modified COC surfaces were imaged by an atomic force microscope (PSIA XE-100, Park Scientific). Image acquisition was accomplished by using a standard Si_3N_4 cantilever in an ambient environment. The scan rate was optimized to reduce hysteresis between forward and backward traces of the cantilever tip. Comparisons were made among randomly selected probe areas (10 μm × 10 μm) on different sample substrates to examine the topography properties. Images were processed by WSxM software (Nanotec Electronica, Spain).

2.4. Device operation

The inlet of a control channel was connected to a nitrogen tank through a pressure control system as described previously [14]. The gas supplied to the control channel built up the pressure inside, and thus the middle PDMS layer deflected to block the fluid channel. PDMS is well known to be permeable to gas, thus the valve operation could result in gas bubbles in the microchannels. As a result, we followed the literature [24] to fill the control channel with water before use, and air bubbles were then eliminated during valve operations.

To demonstrate the function of the microvalves, we introduced two solutions (as dyed in different colors) in a device integrated with two valve arrays. All channels in Fig. 1a were first filled with a red dye solution. After the valve arrays were actuated (closed), the existing solution in the horizontal channel was removed and replaced by a blue dye solution. It is noteworthy to point out that no cross-diffusion between the interconnected channels was detected, showing complete isolation upon the closure of valves. Micrographs were captured by an inverted microscope (Olympus IX71) equipped with a color video camera (JVC TK-128OU).

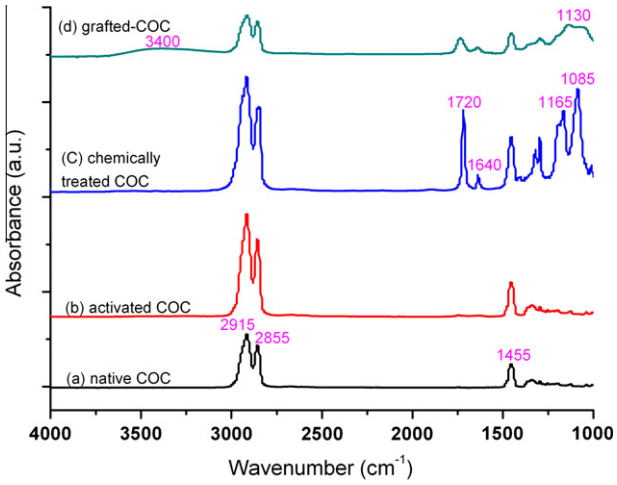

Fig. 2. ATR-FTIR spectra of COC in the native form and those after various surface treatments. (a) Native COC; (b) COC surface activated by corona discharges; (c) COC surface activated and then treated with TMSPMA; and (d) COC surface activated, TMSPMA-treated, and exposed to the second corona discharges, followed by annealing.

3. Results and discussion

3.1. Surface treatment and characterization

Attenuated total reflection Fourier transform infrared (ATR-FTIR) spectroscopy was employed to study the COC surface property after physical and chemical treatment. We obtained the spectra of COC surfaces in the native form and after each step of surface treatment. Fig. 2a shows ATR-FTIR spectrum of the native COC while that of the same surface after activation using corona discharges is in Fig. 2b. Note that ATR-FITR spectra should be obtained immediately after the surface treatment, so that the surface property restoration over time [25] could be avoided. Comparison of the spectra in Fig. 2a and b shows an increase in the signals of the C—H stretches and bending at the wavenumbers of 2915 cm^{-1}, 2855 cm^{-1} and 1455 cm^{-1}. This increase corresponds to a more heterogeneous morphology arising from corona activation (see AFM imaging as discussed below), which yields a larger surface area, and in turn allows a greater contact area when the sample surface is forced in contact with the ATR crystal. Consequently, more evanescent waves from the inferred beam (normally extends beyond the crystal for few microns) could be absorbed by the sample surface, resulting in increased stretching signals in IR spectrum. However, we did not observe a peak around 3400 cm^{-1} associated with the presence OH groups. Several studies on surface treatment using plasma or UV/Ozone suggested the creation of OH groups, though these efforts were on PDMS or PMMA [12,17–19].

After the corona discharge treatment, COC was exposed to 3-(trimethoxysilyl)propyl methacrylate (TMSPMA). After removing unbound reagents, the COC sheet was subjected to ATR-FTIR and the spectrum is shown in Fig. 2c. The sharp peaks of C—O and Si—O bonds at 1165 cm^{-1} and 1085 cm^{-1} suggest the presence of silicon-containing organic molecules on the COC surface [26]. The stretching bands at 1720 cm^{-1} and 1640 cm^{-1} are the characteristics of C=O and C=C bonds in the methacrylate portion of TMSPMA. The chemical structure of TMSPMA is shown in Fig. 3a. For comparison, the chemical structure of APTES is shown in Fig. 3b. APTES was used as a silane agent in the several surface modification studies [15–19] and the major difference between TMSPMA and APTES is the double bonds in methacrylate.

After the chemical treatment, COC surface was exposed to the second dose of corona discharges, followed by annealing at 60 °C overnight. The resulting ATR-FTIR spectrum of the COC surface is shown in Fig. 2d. The Si—O—Si bridge between neighboring monomers and some C—O—C in their pristine ester groups can be taken into account for the broad band around the wavenumber of 1130 cm^{-1}. A wide hump near 3400 cm^{-1} indicates the transformation of some of Si—OCH_3 to Si—OH during this surface modification step. Although the prominent decrease in the peak areas at

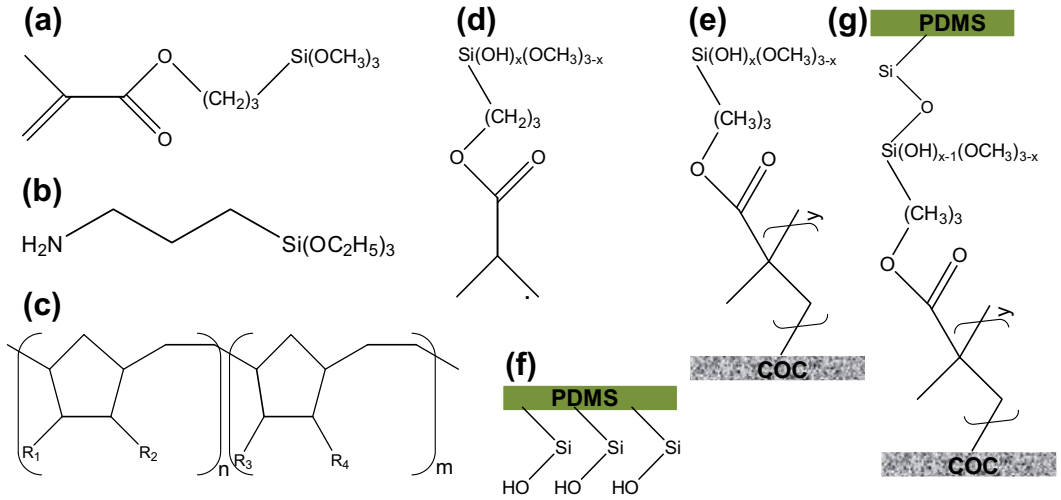

Fig. 3. (a) Chemical structure of 3-(trimethoxysilyl)propyl methacrylate (TMSPMA). (b) Chemical structure of (3-aminopropyl)triethoxysilane (APTES). (c) Chemical structure of Zeonor polymer according to the manufacturer. R_1–R_4 are functional groups while n & m are the number of monomer units in the polymer. (d) Generation of TMSPMA radicals at C=C bond after corona discharges while some Si—OCH_3 were transformed to Si—OH ($x \leqslant 3$). (e) Attachment of TMSPMA to COC through the formation of covalent bond between the radical and C—H groups on the surface via grafting polymerization. (f) Generation of OH groups on PDMS surfaces by activation. (g) Bonding of COC and PDMS through the formation of covalent bond via the dehydration reaction between Si—OH groups on both COC and PDMS surfaces.

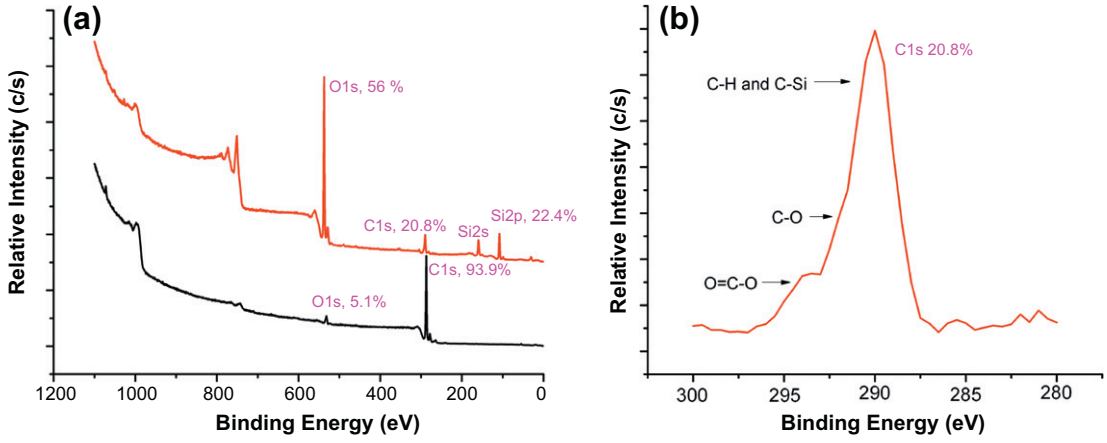

Fig. 4. (a) XPS spectra of native COC (black) and TMSPMA-grafted COC (red). (b) Exploded view of the narrow band of C1s region in the XPS spectrum of the TMSPMA-grafted COC in Fig. 4a. (For interpretation of the references to color in this figure legend, the reader is referred to the web version of this article.)

1720 cm^{-1} and 1640 cm^{-1} indicates the reduction of C=O and C=C double bonds due to reactions to the COC surface and cross-linking among TMSPMA molecules, the appearance of minor peaks at same wavenumbers could result from the residual TMSPMA molecules that were physically entangled in the grafted polymer layer. Besides, the overall decrease in peak intensities is likely due to the ethanol rinse after the second corona-discharge.

3.2. Reaction mechanism and bonding

The ATR-FTIR spectra discussed above led us to propose the reaction mechanism illustrated in Fig. 3. While COC is a saturated hydrocarbon polymer as shown in Fig. 3c, the C=C bonds in the methacrylate moiety of TMSPMA is less stable under the electrical arc induced by the coronal discharge, which has an output ranging from 10 kV to 50 kV according to the manufacturer. Therefore, radicals are likely induced in the TMSPMA coating as shown in Fig. 3d. These radicals would initiate grafting polymerization to the COC substrate, in a way similar to those reported in photo-initiated grafting on a plastic surface [20,21]. The structure after the grafting polymerization process is shown in Fig. 3e.

Sample preparation was completed in the same manner as for FTIR study, followed by XPS analysis. The obtained XPS spectra are shown in Fig. 4a, and we observed a strong peak at 118 eV for Si(2p) on TMSPMA-grafted COC surface. In contrast, there is no Si peak in the XPS spectrum of a native COC surface. This result clearly indicates that TMSPMA molecules have been covalently bonded to the COC surface. In addition, there is a significantly stronger peak at 537.5 eV for O(1s) in the treated COC than in the pristine COC spectrum. The increase is also attributed to the covalent bonding of TMSPMA molecules to the COC surface.

We also observed a large decrease in the C(1s) signal, which indicates partial conversion of Si—OCH_3 to Si—OH as indicated in Fig. 3d and e. The exploded view of this carbon peak is shown in Fig. 4b, and it is resolved into three subtle peaks, unveiling the distinct chemical environments associated with carbon atoms in the scanned area. Despite having a higher composition of carbon than silicon in TMSPMA content, those molecules linked to COC surface through their methacrylate moieties as depicted in Fig. 3e, and this

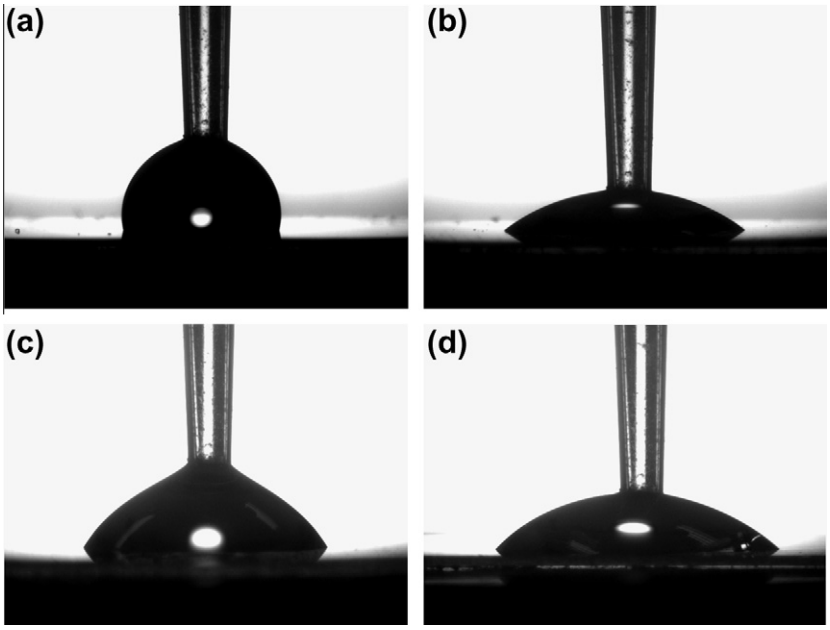

Fig. 5. Pictures of representative water droplets on the surfaces of (a) native COC, (b) corona-discharge-activated COC, (c) TMSPMA-coated COC, and (d) TMSPMA-coated COC after the second corona discharge.

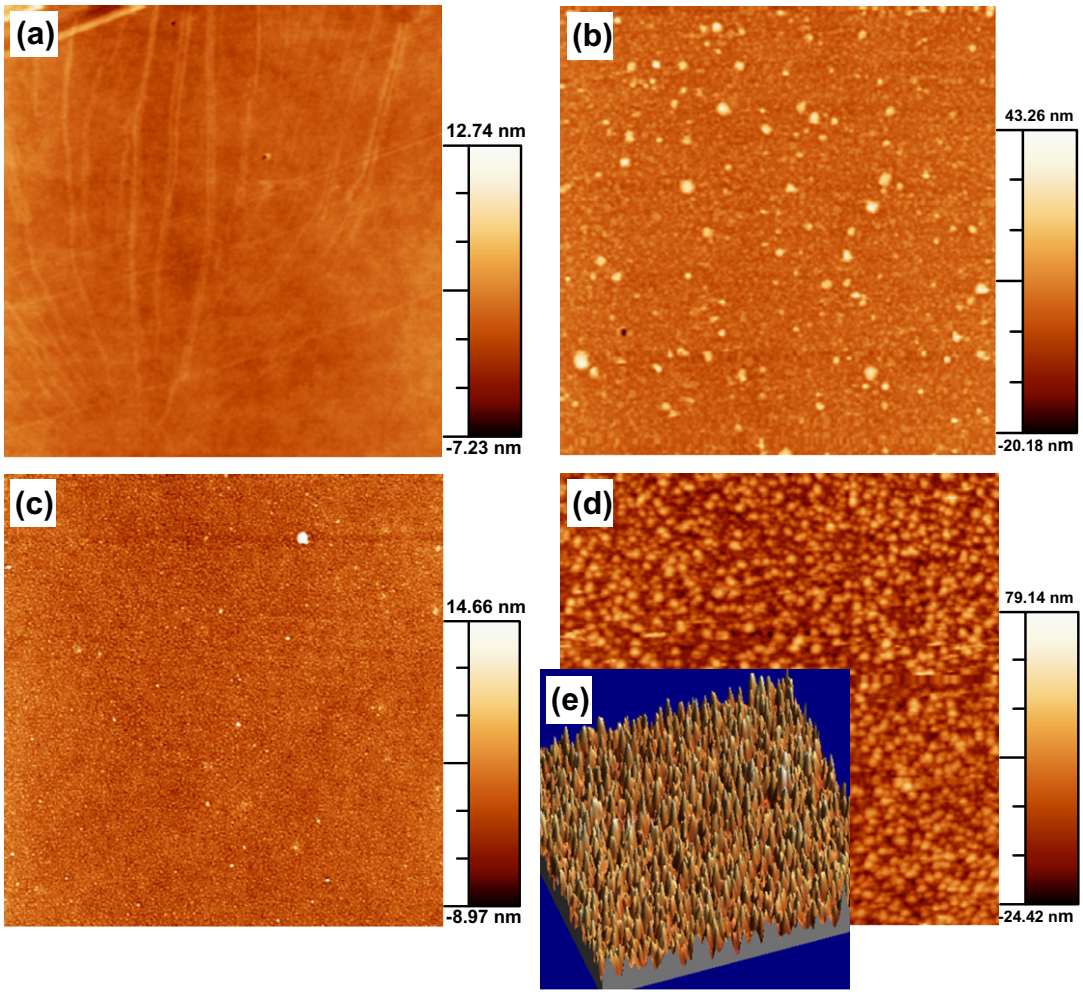

Fig. 6. AFM height images of the surfaces of (a) native COC, (b) corona-discharge-activated COC, (c) activated COC with TMSPMA coating (d) TMSPMA-coated COC after the second corona discharge, and (e) 3-dimensional topographic picture of (d). The height range is indicated by the scale bar. All images were obtained under a dry condition on the surface.

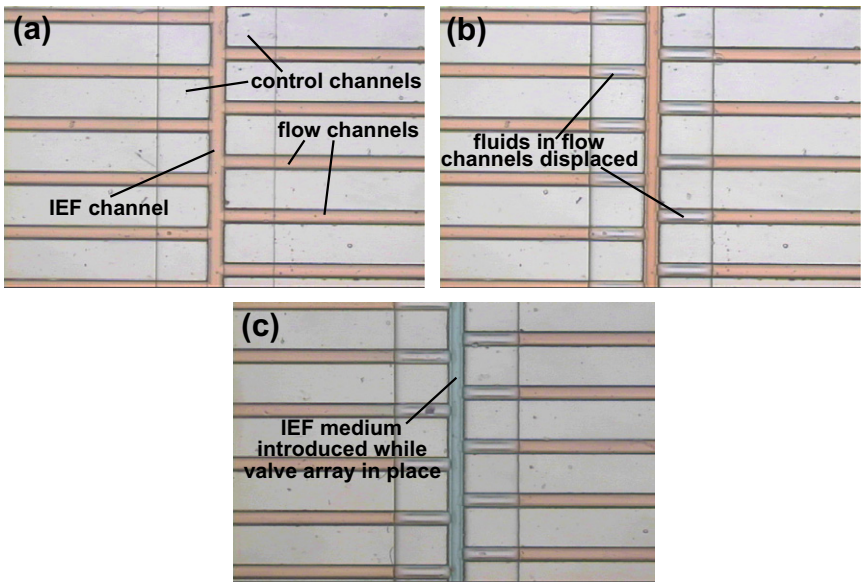

Fig. 7. Photographs of channel intersections showing valves open (a) and closed (b). For easy visualization, a solution of a red food dye was filled in the 39 parallel flow channels (five channels are in the field view of the microscope) and the IEF channel. When the control channel is compressed by a high-pressure N_2 source, the valves were actuated (closed) and the red solution in the valve region was displaced. (c) Photograph of the channel intersections after the solution in the central channel was replaced with another solution (dyed in blue for easy visualization) while valves were closed. (For interpretation of the references to color in this figure legend, the reader is referred to the web version of this article.)

particular orientation might explain the comparable signals of Si(2p) and C(1s) in XPS spectrum of TMSPMA-grafted COC.

The bonding mechanism between the treated COC with PDMS is shown in Fig. 3g while the surface of the activated PDMS is illustrated in Fig. 3f. It is well-studied that silanol groups can be formed on the surface of PDMS via high-energy activation methods such as plasma, UV/ozone treatment, or corona discharges (Fig. 3f) [27–29]. When the activated PDMS surface was placed in contact with the TMSPMA-treated COC, dehydration reactions took place between hydroxyl groups on two surfaces and Si—O—Si bonds were formed (Fig. 3g). An annealing process at a high temperature for a period of time helped complete the dehydration reaction and promote bonding between COC and PDMS.

3.3. Surface wettability and morphology

The effects of the physical and chemical treatment on surface hydrophilicity and wettability were investigated by measuring their contact angles. Fig. 5a and b shows the pictures of representative water droplets on the surfaces of native COC and corona-discharge-activated COC. The mean contact angle on corona-discharge-activated COC surface $(42.2 \pm 0.7)^\circ$ was significantly less than native COC $(100 \pm 1)^\circ$, indicating a notable increase in the hydrophilicity of the COC surface. In essence, the hydrophobic surface of native COC was converted into a hydrophilic surface through the corona discharge treatment, which increased its surface energy and wettability regardless of the changes in surface morphology. It should be reiterated that no hydroxyl groups were generated during this step, as discussed above. The corona-discharge-activated COC surface was then coated with a layer of TMSPMA, followed by the second treatment of corona discharge. The pictures of representative water droplets on their surfaces are shown in Fig. 5c and d. The hydrocarbon chain of TMSPMA makes the surface hydrophobic. However, the additional corona discharge treatment decreased the value of contact angle from $(64 \pm 1)^\circ$ to $(45 \pm 1)^\circ$. This change is mainly attributed to the conversion of functional group from Si—OCH_3 to Si—OH (silanol), although co-occurrence of C—OH groups on the modified surface is possible after the second corona discharge. In addition, the surface wettability, indicated by the changes in contact angle, is in good agreement with the results obtained in the ATR-FTIR study.

The effects of the physical and chemical treatment on surface morphology were investigated by atomic force microscope (AFM). Fig. 6a and b shows the AFM images of the native COC surface and the corona-discharge-activated COC surface. The AFM images clearly show that large morphological changes took place during corona discharge of the COC surface. The native COC sample possesses relatively smooth surfaces (except for a few mechanical wrinkles) whereas the corona-discharge-activated COC surface is coarse with nano-scale features. The root-mean-square (RMS) roughness is evaluated as 1.6 nm and 4.0 nm for the former and the latter, respectively. As a reference, plasma oxidation of PDMS also led to large morphological changes; the oxidized, silica-like surface layer on the PDMS resulted in wavy patterns in AFM images [28,30]. After coating a thin layer of TMSPMA, the activated COC surface was slightly smoothened as shown in Fig. 6c. However, grafting polymerization initiated by the second dose of corona discharge brought out highly heterogeneous morphology as shown in Fig. 6d. Its large RMS roughness of 9.8 nm illustrated in the three-dimensional topographic picture in Fig. 6e manifests the growth of a grafted polymeric layer of TMSPMA on the COC surface.

3.4. Valve operation

As mentioned above, COC/PDMS bonding was developed for fabricating reliable valve arrays. We further exploited the use of valves for fluidic handling and the findings suggested an alternative to gel pseudo valves employed for protein separation [31]. Fig. 1a shows the layout of the device we used for two-dimensional protein separation [22]. The device consists of one AB channel for the first dimension and a number of CD channels for the second dimension. In many circumstances, for example two-dimensional protein separation and enzyme-linked immunosorbent assay (ELISA), different solutions are simultaneously required, thus valve

arrays would be useful to prevent two separation media or different buffers from cross-contaminating at the interface. As shown in Fig. 1b, the valve array is represented by the gray lines on each side of the AB channel. For simple and clear demonstration, reagents used for aforementioned bioanalyses are substituted by color solutions.

To demonstrate the operation of two valve arrays, two control channels were pneumatically controlled using a high-pressure N_2 source, which compressed the PDMS layer to actuate the valves. All channels in the fluid layer were filled with a red dye solution. Fig. 7a shows an exploded-view picture of five channels when valves were open (no pressure in control channels). We then supplied a pressure of 45 psi into the control channels, the valves on the both sides of the IEF channel were closed as indicated in Fig. 7b. The disappearance of the red dye solution in the overlapped region demonstrated the complete valve closing. When the pressure in the control channels was relieved, valve arrays were opened again and the red dye flowed back into the channels. Thus, cyclic operations of valve closing-opening were demonstrated.

As shown in Fig. 7c, after two valve arrays were closed, the red dye solution in the central channel AB was replaced by a blue dye solution. This result indicates that microvalves introduced two types of solutions into orthogonal channels possible without cross-contamination; therefore the established valve function would find its potential use for two-dimensional separation based on different mechanisms [32].

4. Conclusion

A method of bonding COC with PDMS has been developed and it is enabled by corona discharges that activate COC surfaces and induce radicals-initiated grafting polymerization. Each step of the surface modification and bonding has been studied using a number of techniques including ATR-FTIR, XPS, AFM and contact angle measurement. via a C—C covalent bond, TMSPMA is anchored on the COC surfaces. A PDMS membrane with activated surfaces can then be irreversibly sealed to the COC substrate containing microchannels. The bonding method is easy to implement, requiring minimal amount of chemicals and conventional laboratory equipment. The resultant bonding is strong, and the process and results are reproducible. As reported elsewhere [14], the PDMS elastomer valve manufactured by this means was subjected to a pneumatic pressure as high as 100 psi with no delamination was observed. More importantly, the hydrolytic stability of this approach is superior to those of using APTES as an adhesive layer, hence meeting a broader range of microfluidic needs. Further, the bonding method is also applicable to PMMA/PDMS bonding [14].

In addition, we integrated PDMS-based microvalve arrays with a COC-based two-dimensional protein separation device. The robust sealing of the device delivered reliable and repeatable valve actuation when pressures were applied to the microchannels in the device. Two types of media were successfully introduced into orthogonally intersected channels, without cross-contamination, when the valves were in place. The presented valve fabrication method is conventional and accessible for many laboratories, and believed to have increasing relevance for routine lab-on-a-chip processes.

Acknowledgments

This work is supported in part by National Institute of Health (R21RR024397, R21RR026215, and K25CA149080), the Flight Attendant Medical Research Institute (FAMRI-082502), Defense Advanced Research Projects Agency (DARPA) via Micro/Nano Fluidics Fundamentals Focus Center at the University of California at Irvine (HR001-06-1-0500), and the University of Florida via the Research Opportunity Fund. The content is solely the responsibility of the authors and does not necessarily represent the official views of the funding agencies. We would like to thank Major Analytical Instrumentation Center (MAIC) and Particle Engineering Research Center (PERC) at University of Florida for their assistance in AFM, XPS, and contact angle measurement.

References

[1] A. Arora, G. Simone, G.B. Salieb-Beugelaar, J.T. Kim, A. Manz, Anal. Chem. 82 (2010) 4830–4847.
[2] D.J. Harrison, P.G. Glavina, A. Manz, Sens. Actuators B – Chem. 10 (1993) 107–116.
[3] Z.H. Fan, D.J. Harrison, Anal. Chem. 66 (1994) 177–184.
[4] S.C. Jacobson, R. Hergenroder, L.B. Koutny, R.J. Warmack, J.M. Ramsey, Anal. Chem. 66 (1994) 1107–1113.
[5] D.C. Duffy, J.C. McDonald, O.J.A. Schueller, G.M. Whitesides, Anal. Chem. 70 (1998) 4974–4984.
[6] M.A. Unger, H.P. Chou, T. Thorsen, A. Scherer, S.R. Quake, Science 288 (2000) 113–116.
[7] T. Thorsen, S.J. Maerkl, S.R. Quake, Science 298 (2002) 580–584.
[8] P. Yager, T. Edwards, E. Fu, K. Helton, et al., Nature 442 (2006) 412–418.
[9] E.W. Young, E. Berthier, D.J. Guckenberger, E. Sackmann, et al., Anal. Chem. 83 (2011) 1408–1417.
[10] S.J. Clarson, J.A. Semlyen, Siloxane Polymers, Prentice Hall, Englewood Cliffs, NJ, 1993.
[11] K. Pitchaimani, B.C. Sapp, A. Winter, A. Gispanski, et al., Lab Chip 9 (2009) 3082–3087.
[12] W. Zhang, S. Lin, C. Wang, J. Hu, et al., Lab Chip 9 (2009) 3088–3094.
[13] G. Mehta, J. Lee, W. Cha, Y.C. Tung, et al., Anal. Chem. 81 (2009) 3714–3722.
[14] P. Gu, K. Liu, H. Chen, T. Nishida, Z.H. Fan, Anal. Chem. 83 (2011) 446–452.
[15] H. Hwang, H.H. Kim, Y.K. Cho, Lab Chip 11 (2011) 1434–1436.
[16] V. Sunkara, D.K. Park, H. Hwang, R. Chantiwas, et al., Lab Chip 11 (2011) 962–965.
[17] K.S. Lee, R.J. Ram, Lab Chip 9 (2009) 1618–1624.
[18] M.E. Vlachopoulou, A. Tserepi, P. Pavli, P. Argitis, et al., J. Micromech. Microeng. 19 (2009) 015007.
[19] L. Tang, N.Y. Lee, Lab Chip 10 (2010) 1274–1280.
[20] T. Kondo, M. Koyama, H. Kubota, R. Katakai, J. Appl. Polym. Sci. 67 (1998) 2057–2064.
[21] T. Rohr, D.F. Ogletree, F. Svec, J.M.J. Frechet, Adv. Funct. Mater. 13 (2003) 264–270.
[22] C. Das, J. Zhang, N.D. Denslow, Z.H. Fan, Lab Chip 7 (2007) 1806–1812.
[23] C.K. Fredrickson, Z. Xia, C. Das, R. Ferguson, et al., J. Microelectromech. Syst. 15 (2006) 1060–1068.
[24] Y.C. Wang, M.H. Choi, J. Han, Anal. Chem. 76 (2004) 4426–4431.
[25] Y. Li, Z. Wang, L.M. Ou, H.Z. Yu, Anal. Chem. 79 (2007) 426–433.
[26] K. Nakanishi, P.H. Solomon, Infrared Absorption Spectroscopy, Holden Day, San Francisco, 1977.
[27] M.K. Chaudhury, G.M. Whitesides, Langmuir 7 (1991) 1013–1025.
[28] B. Wang, R.D. Oleschuk, J.H. Horton, Langmuir 21 (2005) 1290–1298.
[29] B. Park, S. Song, Biochip J. 1 (2007) 140–143.
[30] D.B.H. Chua, H.T. Ng, S.F.Y. Li, Appl. Phys. Lett. 76 (2000) 721–723.
[31] C. Das, C.K. Fredrickson, Z. Xia, Z.H. Fan, Sens. Actuators a – Phys. 134 (2007) 271–277.
[32] H. Chen, Z.H. Fan, Electrophoresis 30 (2009) 758–765.